# Supplementary Information

## Unimolecular Micellization Strategy for Achieving NIR-II Excited Fluorophores with Enhanced Brightness in Aqueous

Zelong Li[a,#], Na Li[a,#], Sanlin Deng[b], Jinkang Zheng[b], Jian Zou[a], Fan Wu[b], Jian Xiong[b], Qiang Kang[a], Hao Xiao[a], Guilong Wu[b,c], Guodong Chen[b], Xiaofeng Tan[a,b]*, Qinglai Yang[a,b,c]*

[a] Center for Molecular Imaging Probe, Cancer Research Institute, Hengyang Medical School, University of South China, Hengyang, Hunan 421001, China.

[b] Department of Hepatopancreatobiliary Surgery, The First Affiliated Hospital, Hengyang Medical School, University of South China, Hengyang, Hunan, 421001, China.

[c] NHC Key Laboratory of Birth Defect Research and Prevention & MOE Key Lab of Rare Pediatric Disease & Hunan Engineering Research Center for Early Diagnosis and Treatment of Liver Cancer, Hengyang Medical School, University of South China, Hengyang, Hunan, 421001, China.

[#] These authors contributed equally to this work.

*Correspondence to: tanxiaofeng@usc.edu.cn and qingyu513@126.com

# Table of Content

# 1. Supplementary methods

## 1.1. Materials

Alkynyl-PEG-hydroxyl ($PEG_{600}$) was purchased from Yarebio Co., LTD. Intralipid® emulsion was purchased from Sigma-Aldrich. Phosphate-buffered saline (PBS), tetrahydrofuran (THF), toluene, dichloromethane (DCM), and dimethyl formamide (DMF) were purchased from Titan Scientific, Inc. Unless otherwise noted, all chemicals were obtained commercially, and used without further purification. The 7.0 kDa molecular weight cut-off dialysis membrane was purchased from Thermo Fisher Scientific, Inc. The syringe filter hydrophobic PTFE (0.22 μm) was purchased from Titan Scientific, Inc.

## 1.2. Measurements

$^{1}H$ and $^{13}C$ NMR spectra were performed on 500 MHz NMR spectrometers (Bruker AVANCE) using $CDCl_3$. The molecular analysis was performed on AutoflexIII Matrix-assisted laser desorption/ionization (MALDI) time-of-flight (TOF) mass spectrometry (Bruker Daltonics, USA). Ultraviolet-visible-near infrared absorption spectra were recorded on a MAPADA UA-3200S spectrometer. Gel permeation chromatography (GPC) was performed on an Agilent GPC series 1260 infinity with a 10 μm PLgel 600 × 7.5 mm column. THF was used as the mobile phase at a flow rate of 1.0 mL/min at 35 ℃.

## 1.3. Quantum yield test

The fluorescence quantum yield (QY) of the fluorophores was measured by the reported methods previously[1]. The fluorescence spectra in the 1100-1700 nm range were performed with the FLS-980 Edinburgh fluorescence spectrometer under a 1064 nm laser excitation. One 1100-nm long-pass filter (Thorlabs) was used to filter the emitted light. The obtained emission spectra were further corrected by the detector and the filter. The fluorescence QY was determined using the reference fluorophore IR-26 with a known QY of 0.05% ($\Phi_{st}$) in $C_2H_4Cl_2$. η is defined as the refractive index of the solvent. All samples were measured at 25 ℃, and reference fluorophore IR-26 was used at the optical density (OD) value of 0.1 at 1064 nm. The NIR-II fluorescence emission intensities were measured under 1064 nm excitation. The QY values of samples were determined based on three concentrations with OD of 0.08, 0.1, and 0.12 at 1064 nm. The intensity obtained from the InGaAs camera was a spectrally integrated total emission intensity in the 1075-1700 nm region. Using the measured OD at 1064 nm and spectrally integrated fluorescence intensity (F), the QY of samples can be calculated according to the following equation (1):

$$\Phi_x(\lambda) = \Phi_{st}(\lambda) \times \frac{F_x}{F_{st}} \times \frac{A_{st}(\lambda)}{A_x(\lambda)} \times \frac{{\eta_x}^2}{{\eta_{st}}^2} = \Phi_{st}(\lambda) \times \frac{F_x}{F_{st}} \times \frac{1-10^{-OD_{st}(\lambda)}}{1-10^{-OD_x(\lambda)}} \times \frac{{\eta_x}^2}{{\eta_{st}}^2} \quad (1)$$

## 1.4. Fluorophore photo/chemical stability

IR-FCT8CP and ICG were dissolved in PBS, FBS, and water at an OD of 0.20 at 1064 nm. The fluorescence signal was monitored using an NIR17S fluorescence spectrometer under a 1064 nm laser at a power density of 1.0 W/cm$^2$. The average

fluorescence intensity of the region of interest was plotted as a function of time. Additionally, to test the resistance of IR-FCT8CP UIMs to reactive oxygen and sulfur species compared to the commercial ICG. IR-FCT8CP UIMs and ICG (40 μmol/L) were dissolved in $H_2O_2$ and GSH, respectively, and their fluorescence spectra were recorded at 10 minutes.

## 1.5. Determination of critical micelle concentration (CMC)

The CMC value of IR-FCT8CP was determined based on the fluorescence intensity at 1237 nm. Micelle solutions with different concentrations (0.78, 1.56, 3.12, 6.25, 12.5, 25, 50, 100, 200, and 400 μmol/L, 2.0 mL) were stirred at room temperature for 4 hours, and the fluorescence intensity was measured. A curve was plotted with micelle concentration on the x-axis and absorbance on the y-axis. The CMC was determined by identifying the point of a sharp increase in fluorescence intensity[2].

## 1.6. Tissue phantom imaging

Firstly, Intralipid® solution (1%) was chosen as a simulated tissue due to its similar scattering characteristics.[3] Then, a glass capillary tube filled with IR-FCT8CP UIMs and ICG (40 μmol/L, in PBS) was encapsulated for imaging purposes. The capillary tube was then placed under a cylindrical culture dish and covered with varying volumes of Intralipid® solution. To capture images, 1500 or 1000 nm long-pass (LP) filters were used to ensure sufficient signal acquisition (a 1064 nm or 808 nm laser at a power density of 0.25 W/cm$^2$, and an exposure time of 400 or 50 ms, respectively). To assess

penetration depth, the average intensity was measured from the same region of interest (ROI) at different depths.

## 1.7. *In vivo* NIR-II fluorescence imaging

Animal experiments were approved by the University of South China and followed the animal experiment ethics review as well as the health guide for the care and use of laboratory animals. Six-week-old female nude mice were purchased from Hunan SJA Laboratory Animal Co., Ltd. **IR-FCT8CP** UIMs suspended in PBS (200 μL, 500 μM) were injected intravenously into six-week-old female nude mice (n = 3). All NIR-II images were collected on a home-built small animal imaging system with 640×512 pixel 2D InGaAs NIR camera SD640 (Xi 'an Tianying Photoelectric Technology Co., LTD) under 1064 nm laser of power density 0.25 W/cm$^2$ (1200 nm long-pass (LP), 1300 nm LP and 1500 nm LP filters were used respectively). The obtained images were analyzed with the ImageJ software.

## 1.8. Biological safety assessment

Blood biochemistry and routine blood analysis were comprehensively performed to investigate the long-term biotoxicity of the UIMs. Blood samples from the three groups were collected on day 14. Hepatic and kidney function parameters, including alkaline phosphatase (ALP), aspartate aminotransferase (AST), alanine transaminase (ALT), creatinine (CREA), blood urea nitrogen (BUN), and uric acid (UA), were monitored. For the routine blood analysis, indices such as white blood cells (WBC), red blood cells (RBC), and granulocytes (Gran) were evaluated. Blood routine examination and

biochemical indices were analyzed using a hematology analyzer. Histopathological analyses of normal organs (liver, lungs, spleen, heart, and kidneys) were also conducted using H&E staining after 14 days[4].

## 1.9. Density functional theory calculations

All the calculations were performed using the Gaussian 09 software[5]. IR-FCD was reported previously[6]. The ground-state ($S_0$) geometries of the simplified structures IR-FCT were firstly optimized using the B3LYP/6-31G(d) method and re-optimized at the tuned-ωB97XD*/6-31G(d) level[7-9]. The corresponding range-separation parameter (ω, in Bohr−1) for each molecule was optimally tuned according to the GAP-tuning method and listed in Table 1. The excited-state ($S_1$) geometries of these molecules were optimized using time time-dependent (TD)-ωB97XD*/6-31G(d) method. The HOMOs and LUMOs, absorption excitation energies of these molecules were obtained at the ωB97XD*/6-31G(d) level based on their optimized $S_0$ geometries. The emission energies of these molecules were calculated at the TD-ωB97XD*/6-31G(d) level based on their optimized $S_1$ geometries.

## 1.10. Molecular dynamics simulations

For each molecule, the structure was optimized with the Gaussian 09 program at the HF/6-31G* level, and then restrained electrostatic potential (RESP) charges and the General Amber Force Field (GAFF) were assigned for the optimized structure.[1] The initial structure was immersed in the center of a truncated octahedral box of TIP3P water molecules, and all of the peptide atoms were no less than 10 Å from the boundary

of the water box. Counterions were added to neutralize the system. To remove bad contacts before the simulation, 8000 steps of steepest descent followed by 2000 steps of conjugate gradient energy minimizations were carried out. The relaxed structure was then gently heated from 0 to 300 K at 50 ps and equilibrated for 50 ps with weak restraints on each molecule, which was equilibrated for another 500 ps at constant pressure without restraint. Production simulations were extended to 10 ns for each molecule, and trajectories were saved every 10 ps. All bonds with hydrogen atoms were fixed using the SHAKE algorithm.

## 1.11. Calculation of molecular dimensions

In this study, the molecular dimensions were calculated using GROMACS tools, including gmx distance, gmx sasa, and gmx gyrate[10-12]. First, the gmx distance was used to calculate distances between specific atom groups within the molecule to analyze the spatial arrangement of particular functional groups. Next, the solvent accessible surface area (SASA) was computed using the gmx sasa tool to characterize the interaction interface between molecules and solvent. Lastly, the radius of gyration (Rg) was calculated using gmx gyrate to indicate the compactness and spatial expansion of molecular conformations. These analyses were performed based on GROMACS trajectory files, with all relevant parameters set to default values.

## 1.12. Calculation of interaction energies

To further investigate intermolecular interactions, interaction energies, including van der Waals and electrostatic energies, were calculated using the gmx energy tool in the

GROMACS package.[6, 12, 13] Specifically, energy data were saved to an energy file (edr file) during simulations. Then, gmx energy was used to extract and analyze relevant energy terms, such as van der Waals interactions (LJ-SR) and electrostatic interactions (Coul-SR). The results were analyzed and plotted as energy versus simulation time to elucidate the interaction characteristics and stability of the molecular systems.

## 1.13. Synthetic procedures and characterization

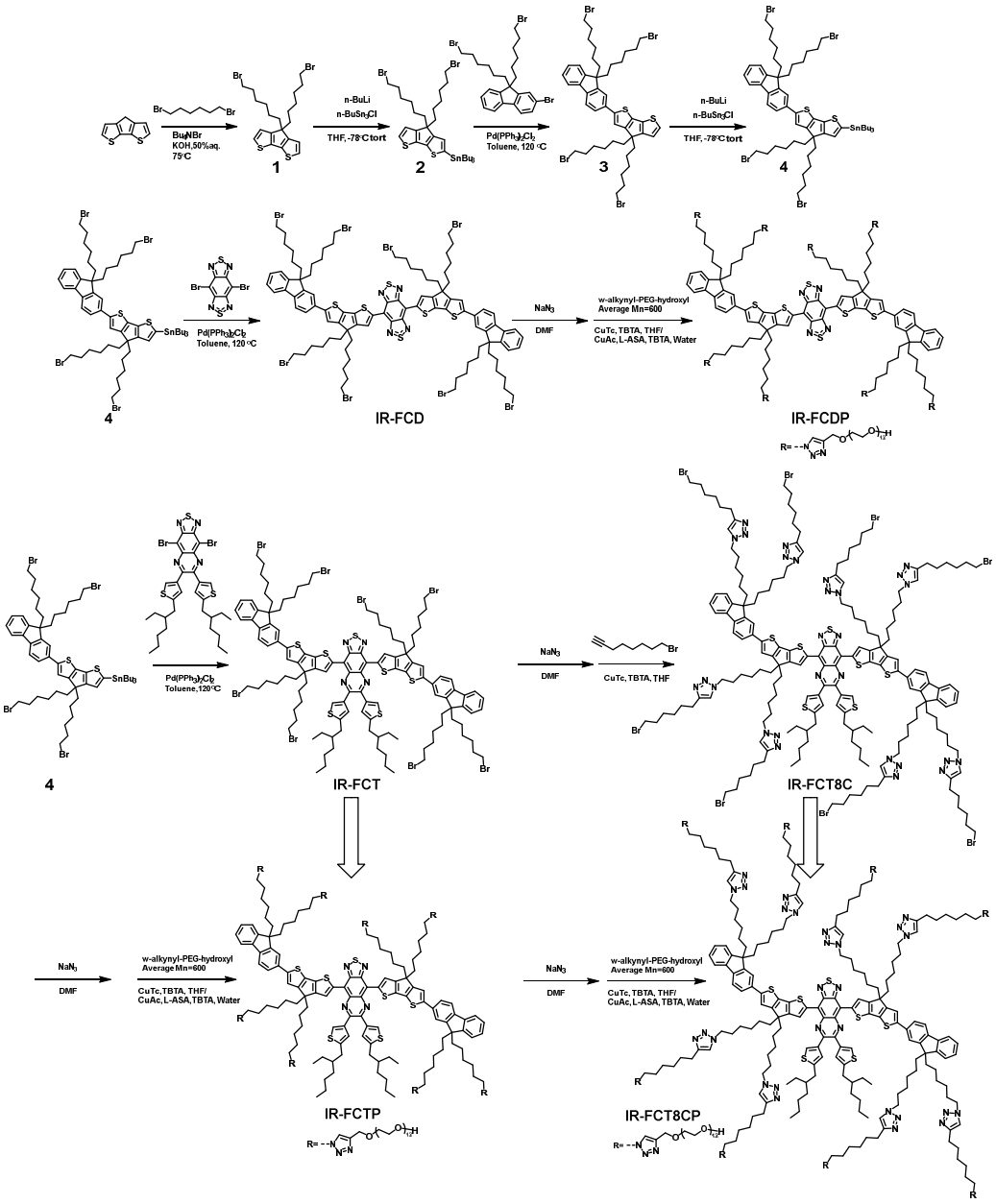

**Supplementary Fig. 1** The detailed synthetic routes of the IR-FCDP, IR-FCTP, and IR-FCT8CP

**Synthesis of Compound 1**

4H-Cyclopenta (2,1-b:3,4-b') dithiophene (2.00 g, 11.22 mmol) and 1,6-dibromohexane (10.95 g, 44.88 mmol) were added to a 250 mL single-necked flask, followed by the addition of 100 mL of 50% w/w KOH solution, and then $Bu_4NBr$ (0.39 g, 1.22 mmol). The mixture was stirred under a nitrogen atmosphere at 75 ℃ for 3 h. After the reaction, the mixture was returned to room temperature, poured into water, and extracted twice with ethyl acetate. The combined organic phase was dried over anhydrous sodium sulfate, and the resulting product was purified by column chromatography on silica gel to obtain **compound 1** as a light brown oil (4.7 g, 83.1%). Characterization data were consistent with previously reported literature data.[6] $^1$H NMR (500 MHz, $CDCl_3$) δ 7.18 (d, J = 4.9 Hz, 2H), 6.94 (d, J = 4.8 Hz, 2H), 3.35 (t, J = 6.8 Hz, 4H), 1.91 – 1.82 (m, 4H), 1.75 (p, J = 7.0 Hz, 4H), 1.33 – 1.27 (m, 4H), 1.16 (p, J = 7.5 Hz, 4H), 0.99 – 0.91 (m, 4H). $^{13}$C NMR (126 MHz, $CDCl_3$) δ: 157.72, 136.62, 124.70, 121.51, 53.12, 37.73, 34.00, 32.68, 29.06, 27.90, 24.26.

**Synthesis of Compound 2**

A flame-dried round-bottom flask under $N_2$ was added **compound 1** (2.50 g, 4.98 mmol) followed by anhydrous THF (15.00 mL). The reaction was then cooled to -78 ℃ and n-BuLi (2.50 M, 2.08 mL, 5.22 mmol) was added dropwise over 10 minutes, and the reaction was allowed to stir for 2 h. Tri-n-butyltin chloride (1.70 g, 5.23 mmol) was then added dropwise, and the reaction was allowed to stir at -78 ℃ for another hour

and subsequently allowed to come to room temperature and stir over another 2 hours. The reaction was then quenched with water, extracted twice with ethyl acetate, and the combined organic phases were dried over anhydrous sodium sulfate and vacuum evaporated to obtain **compound 2**.

**Synthesis of Compound 3**

The obtained stannylated product of **compound 2** (3.00 mmol) was added to 2-bromo-9,9-bis(6-bromohexyl)-9H-fluorene (2.00 g, 3.52 mmol) in a 100 mL single-necked flask. Under a nitrogen atmosphere, Pd $(PPh_3)_4$ (200 mg) was added, followed by the addition of 40 mL of dried toluene solvent. The mixture was stirred at 130 ℃ for 6 h. Then, the mixture was cooled to room temperature and passed through a short pad of silica gel using 1:1 PE/DCM to yield the crude product. The crude product was purified by column chromatography using PE/DCM (5:1) as eluent to yield pure **compound 3**, a yellow-brown solid (1.80 g, 60.3%). Characterization data were consistent with previously reported literature data[6]. $^1$H NMR (500 MHz, $CDCl_3$) δ 7.70 – 7.66 (m, 2H), 7.61 (dd, J = 7.9, 1.7 Hz, 1H), 7.54 (d, J = 1.8 Hz, 1H), 7.35 – 7.29 (m, 3H), 7.25 (s, 1H), 7.18 (d, J = 4.8 Hz, 1H), 6.94 (d, J = 4.9 Hz, 1H), 3.32 (t, J = 6.8 Hz, 4H), 3.26 (t, J = 6.8 Hz, 4H), 2.01 (p, J = 7.4 Hz, 4H), 1.89 (p, J = 6.9 Hz, 4H), 1.73 (p, J = 6.9 Hz, 4H), 1.64 (p, J = 6.9 Hz, 4H), 1.35 – 1.26 (m, 6H), 1.18 (h, J = 7.4 Hz, 6H), 1.13 – 1.03 (m, 6H), 0.97 – 0.83 (m, 6H). $^{13}$C NMR (126 MHz, $CDCl_3$) δ 158.70, 157.41, 151.31, 150.44, 145.01, 140.71, 140.40, 136.86, 135.89, 134.12, 127.18, 127.02, 125.11, 124.26, 122.82, 121.59, 120.23, 119.75, 119.14, 117.32, 55.08, 53.67,

45.14, 40.28, 37.84, 35.47, 35.05, 34.05, 32.73, 32.66, 31.98, 29.14, 29.07, 28.32, 27.93, 27.77, 26.83, 26.65, 26.49, 24.35, 23.55, 23.02, 22.73, 17.35, 14.20, 13.67.

**Synthesis of Compound 4**

The obtained **compound 3** (1.80 g, 1.81 mmol) was added into a flame dried round bottom flask under $N_2$, and followed by anhydrous THF (15.00 mL). The reaction was then cooled to -78 ℃, and n-BuLi (2.50 M, 1.69 mL, 2.71 mmol) was added dropwise over 10 minutes, and the reaction was allowed to stir for 2 h. Tri-n-butyltin chloride (0.88 g, 2.71 mmol) was then added dropwise, and the reaction was allowed to stir at -78 ℃ for another hour and subsequently allowed to come to room temperature and stir over another 2 hours. The reaction was then quenched with water, extracted twice with ethyl acetate, and the combined organic phases were dried over anhydrous sodium sulfate and vacuum evaporated to obtain **compound 4**.

**Synthesis of IR-FCD**

**IR-FCD** was synthesized according to the reference. [6]

**Synthesis of IR-FCT**

The tin-containing product of **compound 4** obtained was combined with 4,9-dibromo-6,7-bis (5-(2-ethylhexyl) thiophen-3-yl)-[1,2,5] thiadiazolo [3,4-g] quinoxaline (TQT) (734 mg, 1 mmol) in a 100 mL single-necked flask. Under a nitrogen atmosphere, Pd $(PPh_3)_2Cl_2$ (150 mg) was added, followed by the addition of 40 mL of dried toluene solvent. The mixture was stirred at 130 ℃ for 6 h, then cooled to room temperature. The mixture was poured into water and extracted with ethyl acetate twice.

The combined organic phases were dried over anhydrous magnesium sulfate. The crude product was purified by column chromatography using PE/DCM (2:1) to yield **IR-FCT**, a dark brown solid (1.8 g, 70%). $^{1}$H NMR (500 MHz, $CDCl_3$) δ 9.06 (s, 2H), 7.80 – 7.65 (m, 6H), 7.60 (s, 2H), 7.52 (d, J = 3.7 Hz, 2H), 7.33 (hept, J = 6.9 Hz, 8H), 6.80 (d, J = 3.7 Hz, 2H), 3.42 (dt, J = 13.4, 6.7 Hz, 1H), 3.29 (dt, J = 13.3, 6.8 Hz, 1H), 2.94 (d, J = 6.8 Hz, 4H), 2.17 – 2.01 (m, 16H), 1.66 (h, J = 6.8 Hz, 10H), 1.61 – 1.49 (m, 8H), 1.46 – 1.30 (m, 16H), 1.30 – 1.08 (m, 46H), 1.04 (t, J = 7.4 Hz, 6H), 0.94 (t, J = 7.0 Hz, 6H). $^{13}$C NMR (126 MHz, $CDCl_3$) δ 158.06, 151.07, 150.47, 149.19, 145.48, 145.30, 140.71, 139.33, 134.27, 131.65, 127.26, 127.07, 124.81, 124.41, 124.02, 123.52, 122.84, 120.30, 119.81, 119.05, 118.90, 114.13, 55.13, 45.16, 41.76, 40.35, 38.21, 34.73, 34.05, 34.01, 32.76, 32.67, 32.60, 31.97, 31.55, 30.18, 29.75, 29.41, 29.25, 29.11, 29.01, 27.96, 27.80, 25.92, 24.49, 23.58, 23.13, 22.74, 14.31, 14.19, 11.20. MALDI-TOF MS (m/z): [$C_{124}H_{151}Br_8N_4S_7$] calcd. 2559.4; found 2559.9.

**Synthesis of IR-FCT8C**

**Compound IR-FCT** (100 mg, 0.039 mmol) and sodium azide (50 mg, 0.75 mmol) were dissolved in DMF (10 mL) and heated for 3 h at 70 ℃. Then, a large amount of water was added until all solids were dissolved. The reaction was extracted twice with ethyl acetate, the combined organic phase was dried with $Na_2SO_4$, and evaporated in vacuo. The crude product was subjected to flash column chromatography on silica gel to afford a dark brown solid (90 mg). The dark brown solid was dissolved in THF (5 mL), and copper (I) thiophene-2-carboxylate (CuTc) (3.7 mg), 8-bromo-1-octyne (66mg, 0.35mmol) and tris[(1-benzyl-1H-1,2,3-triazol-4-yl) methyl] amine (TBTA)

(0.1 mM, 20 μL) were added. The system was stirred at RT for 4 h, and then filtered with diatomite to remove CuTc, and the solution was evaporated in vacuo. The crude product was purified by thin layer chromatography using PE/DCM (2:1) to yield **IR-FCT8C**, a dark brown solid (106 mg, 80%). $^{1}$H NMR (500 MHz, $CDCl_3$) δ 9.06 (s, 2H), 7.89 – 7.65 (m, 6H), 7.51 (d, J = 3.7 Hz, 2H), 7.42 – 7.29 (m, 8H), 7.15 (d, J = 9.6 Hz, 8H), 6.82 (d, J = 3.8 Hz, 2H), 4.25 – 4.11 (m, 16H), 3.38 – 3.33 (m, 16H), 2.63 (dt, J = 32.9, 7.7 Hz, 16H), 2.10 – 1.97 (m, 16H), 1.87 – 1.72 (m, 26H), 1.65 (m, J = 22.5, 14.9, 7.2 Hz, 26H), 1.41 – 1.23 (m, 80H), 1.14 – 1.00 (m, 30H), 0.91 (dt, J = 26.8, 7.0 Hz, 12H). $^{13}$C NMR (126 MHz, $CDCl_3$) δ 151.13, 147.94, 145.45, 139.29, 139.13, 138.93, 131.75, 126.23, 124.78, 124.47, 124.37, 123.48, 122.84, 120.41, 119.10, 119.01, 118.87, 114.08, 60.40, 55.09, 50.03, 41.73, 40.31, 38.16, 32.61, 31.93, 31.52, 30.20, 29.70, 29.36 (d, J = 2.4 Hz), 29.25, 28.28, 27.84, 26.99, 26.27, 26.17, 25.89, 25.51, 25.48, 24.43, 23.57, 23.08, 22.70, 14.28, 14.22, 14.15, 11.19. MALDI-TOF MS (m/z): [$C_{188}H_{255}Br_8N_{28}S_7$] calcd. 3770.2; found 3769.9.

**Synthesis of IR-FCDP, IR-FCTP, and IR-FCT8CP**

All compounds were synthesized by the same method. Taking **IR-FCT8CP** as an example, **Compound IR-FCTBC** (100 mg, 0.026 mmol) and sodium azide (50 mg, 0.75 mmol) were dissolved in DMF (10 mL) and heated for 3 h at 70 ℃. Then, a large amount of water was added until all solids were dissolved. The reaction was extracted twice with ethyl acetate, the combined organic phase was dried with $Na_2SO_4$, and evaporated in vacuo. The crude product was subjected to flash column chromatography

on silica gel to afford a dark brown solid (86 mg). The dark brown solid was dissolved in THF (5 mL), and CuTc (3 mg), w-alkynyl-PEG-hydroxyl PEG 600 (Mn = 600) (140 mg), and TBTA (0.1 mM, 20 μL) were added. The product with dark brown solid was obtained after lyophilization. The system was stirred at room temperature for 4 h, then filtered through diatomite to remove CuTc. The resulting solution was recrystallized in methyl tert-butyl ether, yielding a dark brown solid. The dark brown solid was ultrasonically dissolved in 10 mL of water and filtered through a 0.22 μm hydrophilic filter to remove undissolved impurities. The filtered liquid was transferred to a 100 mL single-neck flask. Then, w-alkynyl-PEG-hydroxyl PEG 600 (50 mg) was added, followed by the addition of cupric acetate (CuAc, 3.2 mg) and L-ascorbic acid sodium salt (L-ASA, 7 mg), each dissolved in 2 mL of water. The two solutions were mixed, quickly added to the reaction system, and TBTA (0.1 mM, 20 μL) was added. The mixture was heated to 70°C and reacted for 3 hours. After the reaction, the solution was dialyzed using a 7.0 kDa dialysis membrane to remove unnecessary reaction materials. The resulting dark brown solid, **IR-FCT8CP,** was obtained after lyophilization. GPC measured IR-FCD8P: Mn=7235, PDI=1.06; IR-FCT8P: Mn=7817, PDI=1.13; IR-FCT8CP: Mn=9926, PDI=1.09.

## 2. Supplementary Figures

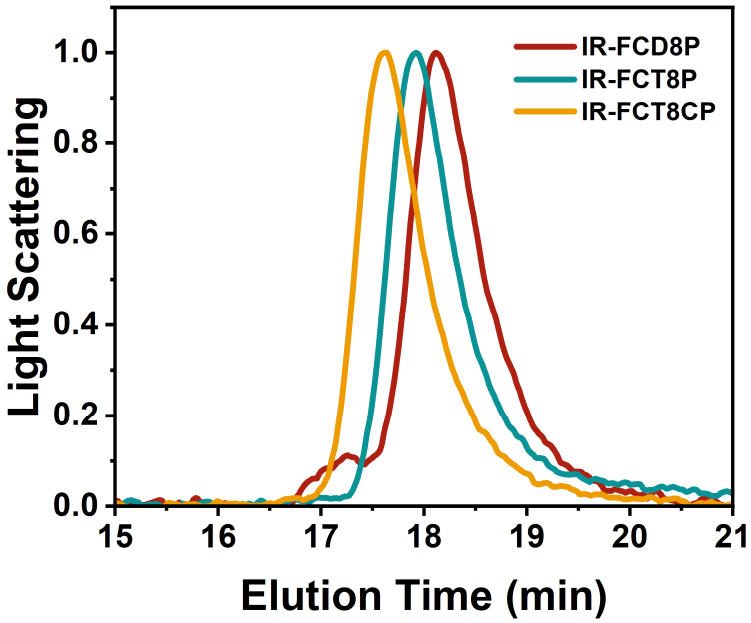


**Supplementary Fig. 2. GPC traces of races of the fluorophores (IR-FCT8CP, IR-FCTP, and IR-FCDP).**

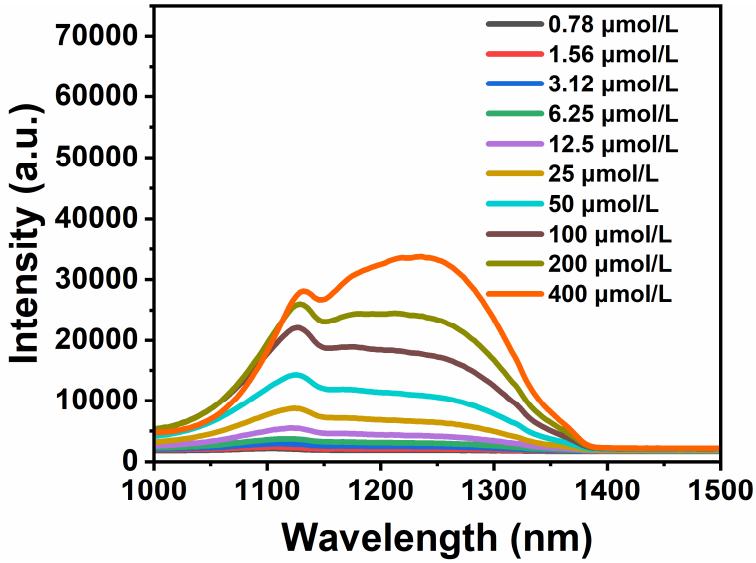


**Supplementary Fig. 3. Fluorescence intensity of IR-FCT8CP UIMs at different concentrations.** The fluorescence intensity values of IR-FCT8CP UIMs at different concentrations (0.78, 1.56, 3.12, 6.25, 12.5, 25, 50, 100, 200, and 400 μmol/L)

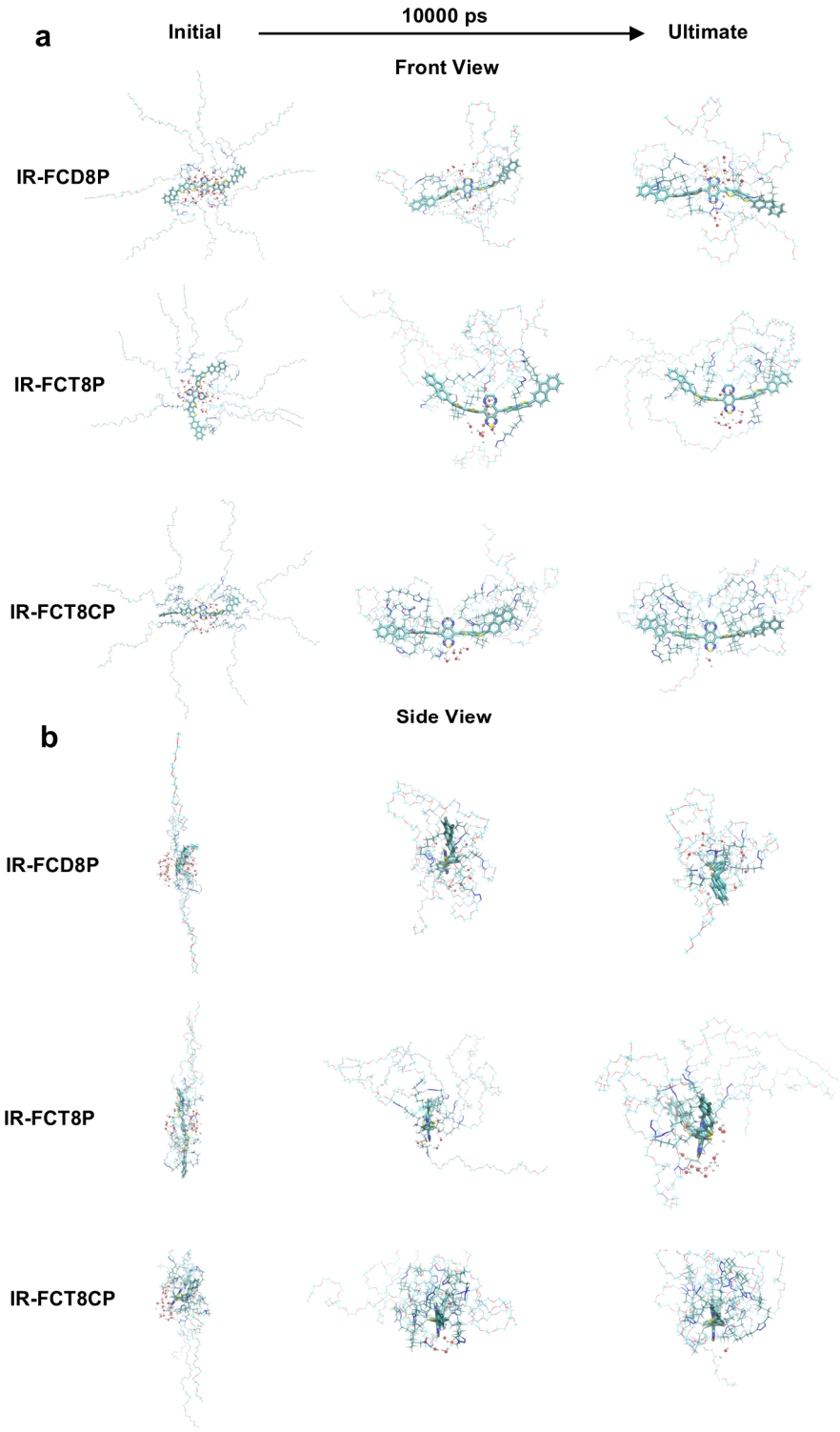


**Supplementary Fig. 4 Representative schematic diagram of water molecules surrounding the molecular fluorophores. a**, Front view. **b**, Side view.

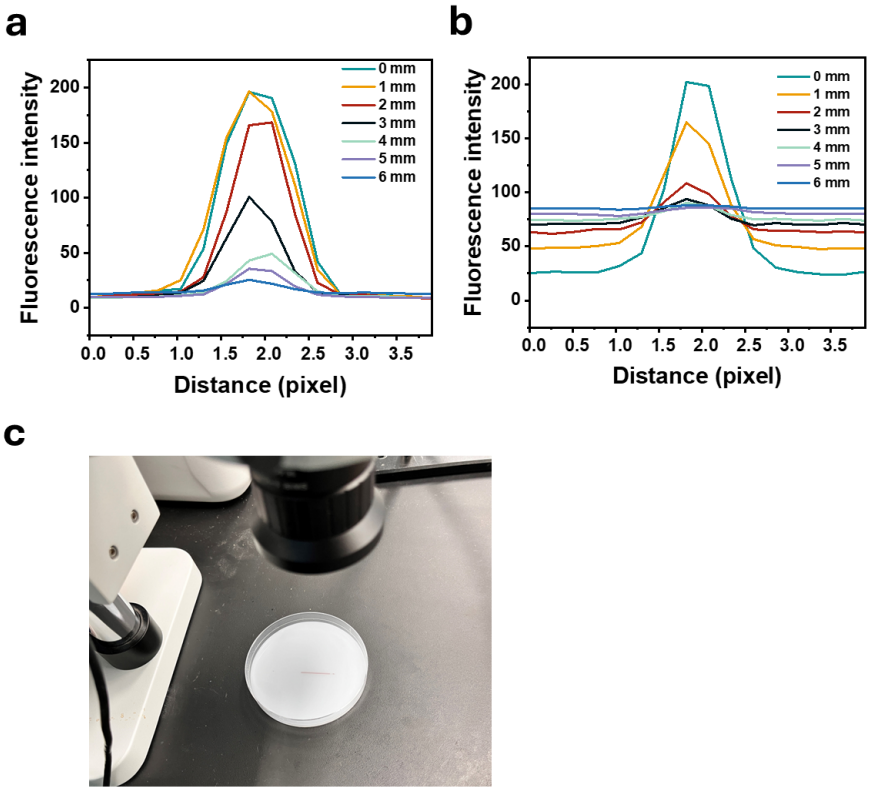


**Supplementary Fig. 5. Evaluation of penetration depth and SBR (Signal-to-Background Ratio). a-b**, Corresponding cross-sectional fluorescence intensity profiles along the pictures were evaluated for IR-FCT8CP UIMs and ICG at each depth. **c**, Bright field top view.

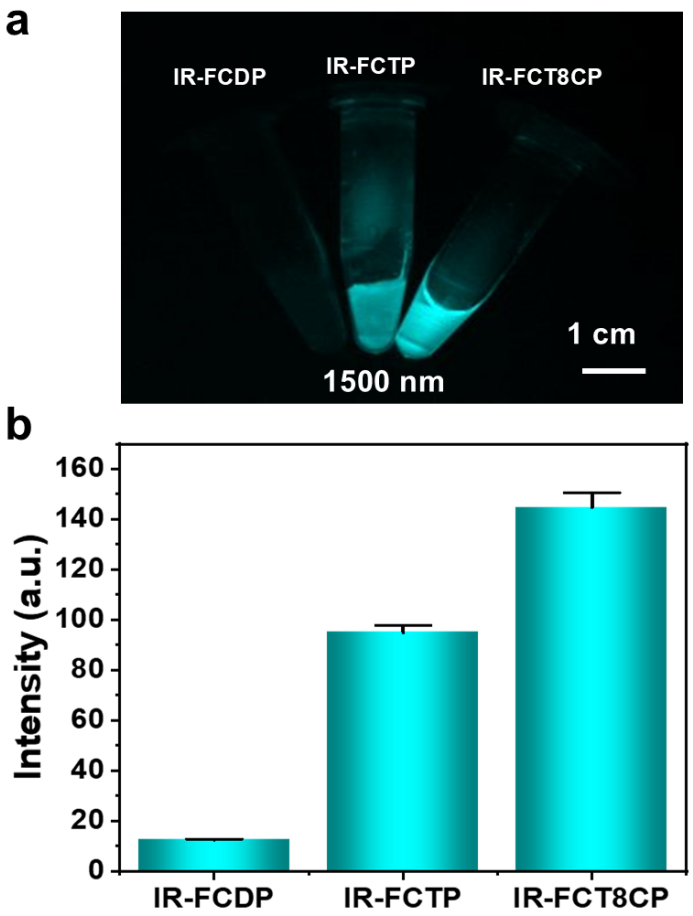


**Supplementary Fig. 6. In vitro imaging. a-b**, The imaging and relative intensity of IR-FCDP, IR-FCTP, and IR-FCT8CP UIMs at NIR-IIb windows under 1064 lasers (n = 3).

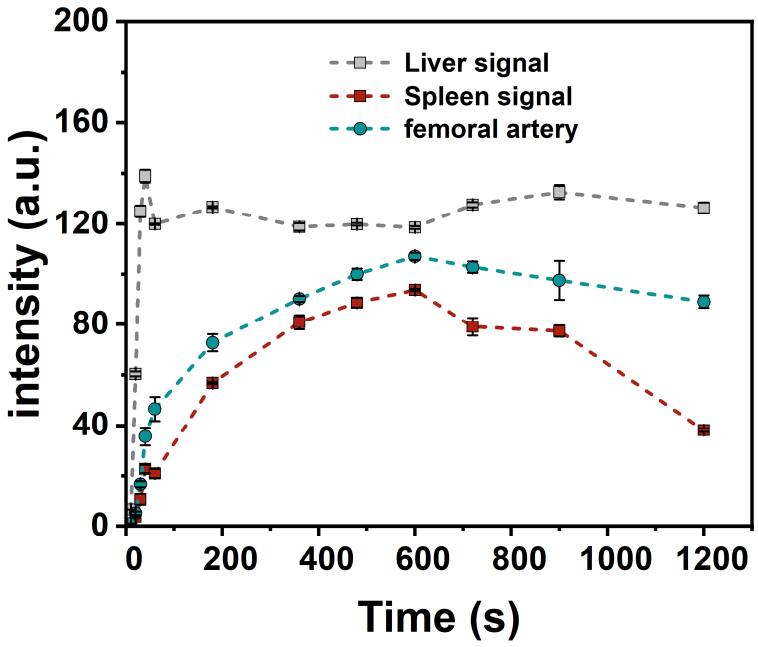


**Supplementary Fig. 7. Half-life of fluorescence signal.** The signal intensities of mice hindlimb vessels, liver, and spleen, were integrated and plotted as a function of time.

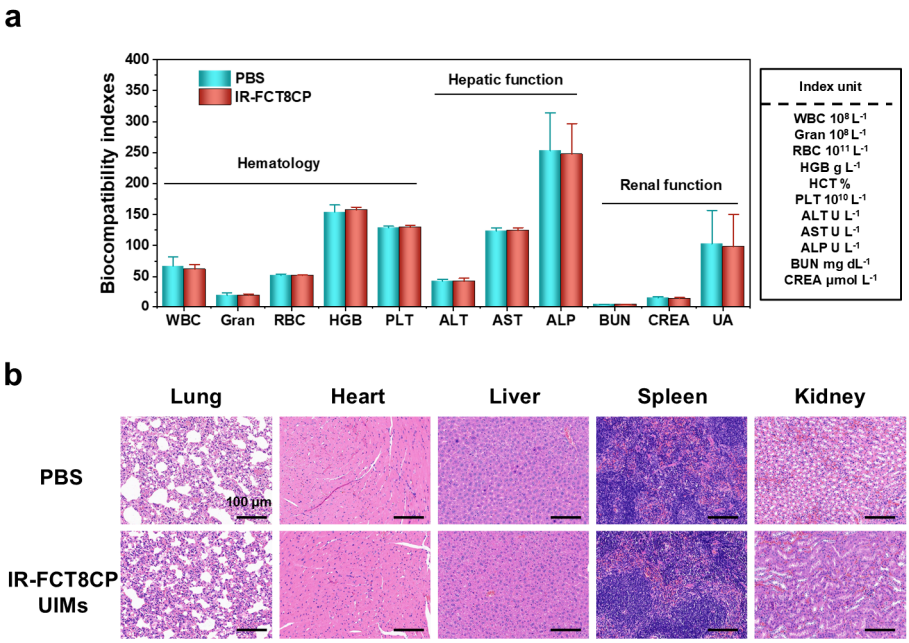


**Supplementary Fig. 8. Biosafety Assessment. a**, Blood routine examination and biochemical assessment of liver function and renal function tests in healthy mice 15 days after injection of different materials. Error bars: mean ± SD (n=3). **b**, H&E staining images of five major organs (heart, liver, spleen, lung, and kidney) after different treatments without 808 nm laser in healthy mice. Scale bar: 100 μm.

## 3. Supplementary Tables

**Supplementary Table 1.** Calculated first vertical $S_0$-$S_1$ excitation energies ($E_{01}$), first vertical $S_1$-$S_0$ emission energies ($E_{10}$), electronic configurations, and reorganization energies determined at the TD-ωB97XD*/6-31G (d) level of theory in vacuum.

| | | Absorption ($S_0 \rightarrow S_1$) | | | Emission ($S_1 \rightarrow S_0$) | | | |
|---|---|---|---|---|---|---|---|---|
| Compound | ω* | $E_{01}$ eV (nm) | $f_{01}$ | Elec. Config. | $E_{10}$ eV (nm) | $f_{10}$ | Reorganization energy (nm) Exp | $K_r$ |
| IR-FCT | 0.13 | 1.22 (1014) | 0.68 | H→L 100% | 0.9763 (1270) | 0.59 | 0.24 (256) | $2.44*10^7$ |
| IR-FCD | 0.118 | 1.14 (1080) | 1 | H→L 100% | 0.9171 (1352) | 0.83 | 0.22 (272) | $3.03*10^7$ |

The reorganization energies are obtained as $E_{01}$ minus $E_{10}$. Note that the experimental reorganization energies measured in weak polar toluene solvent are also listed. $K_r = f_{10}*E_{10}\text{^}2/1.499$, $QY = k_r/k_r + k_{nr}$, where $k_r$ is the radiative decay rate, and $k_{nr}$ is the nonradiative decay rate.

## 4. Supplementary NMR and MALDI-TOF mass spectra

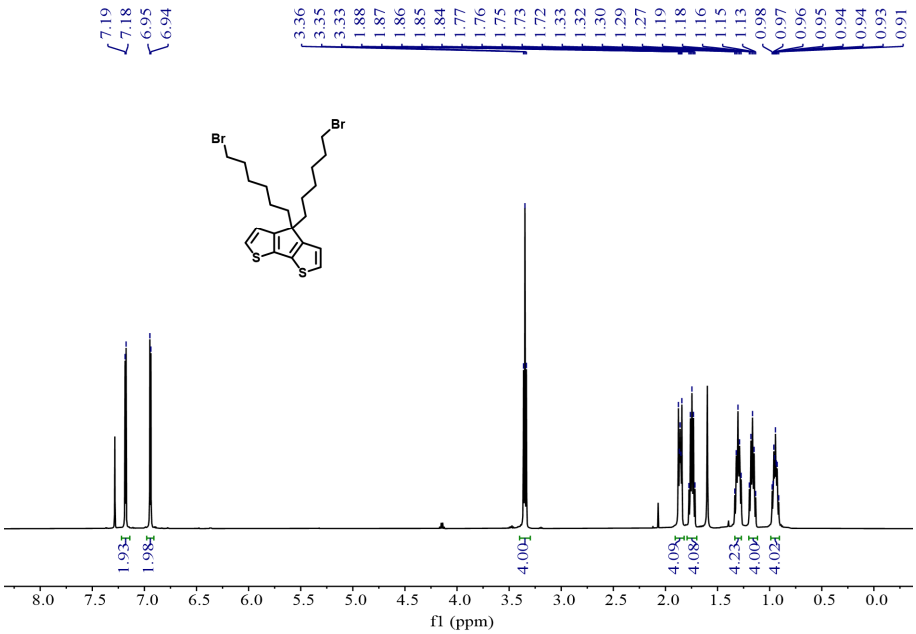


**Supplementary Fig. 9** $^{1}$H NMR spectrum of the **compound 1.**

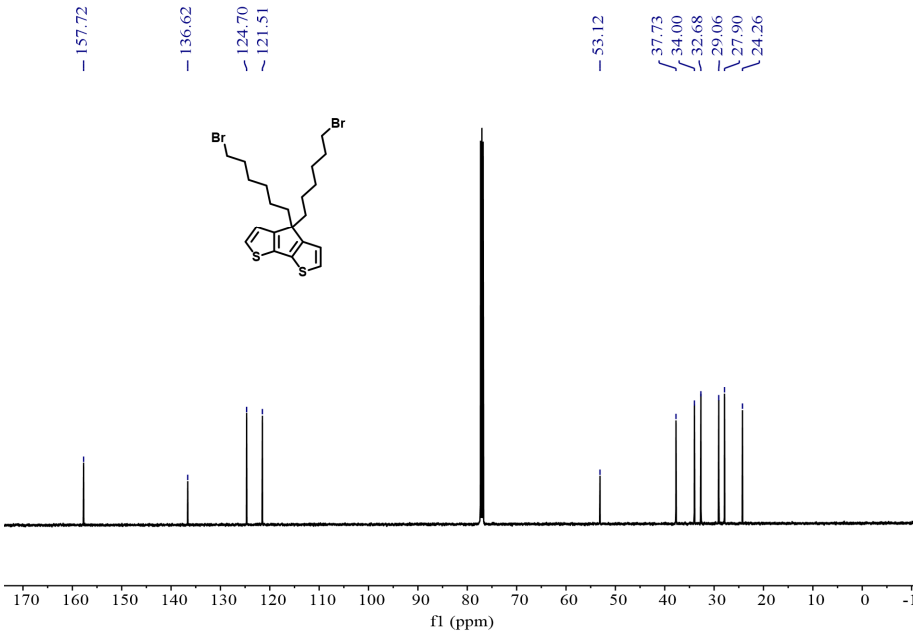


**Supplementary Fig. 10.** $^{13}$C NMR spectrum of the **compound 1.**

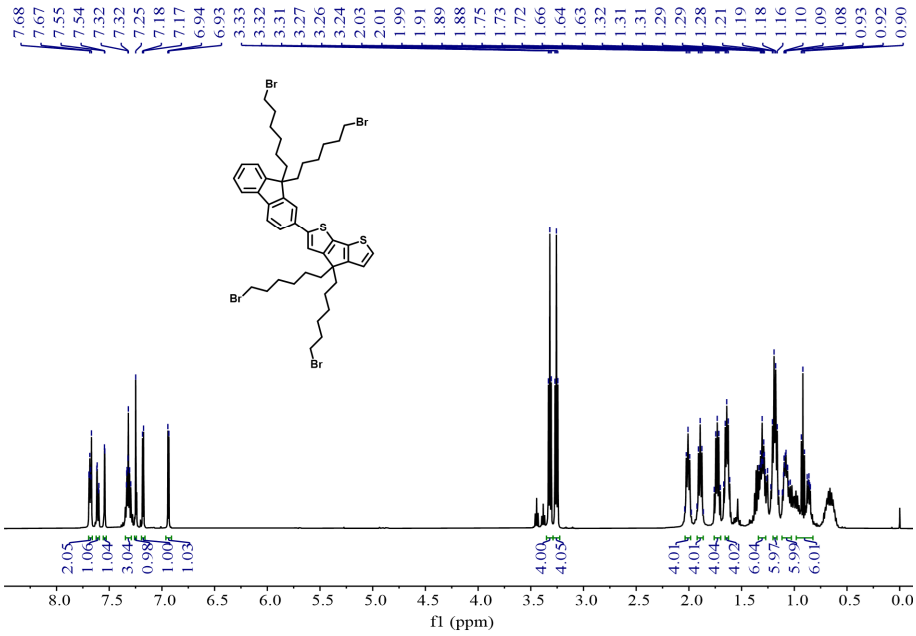


**Supplementary Fig. 11** $^{1}$H NMR spectrum of **compound 3**.

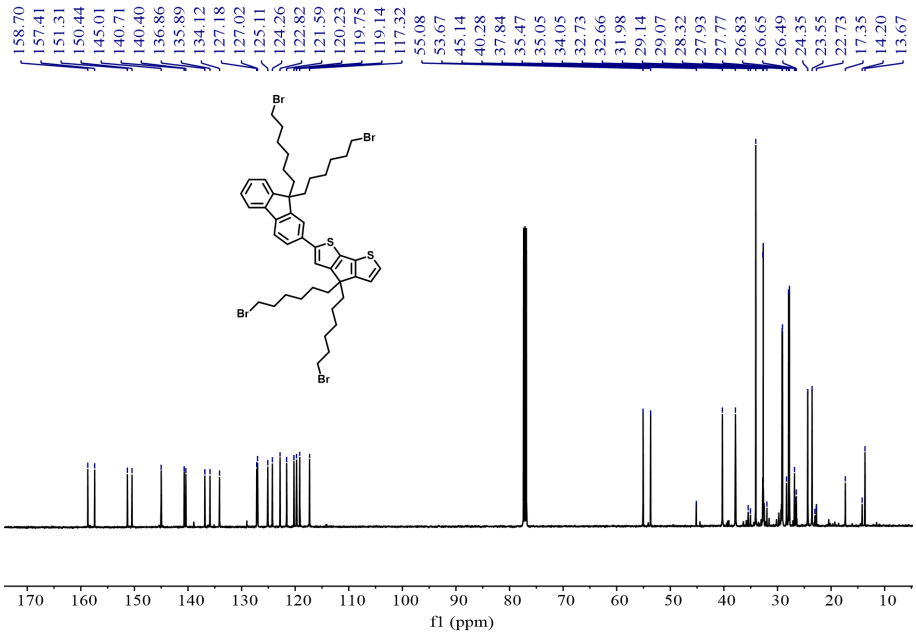


**Supplementary Fig. 12.** $^{13}C$ NMR spectrum of **compound 3**.

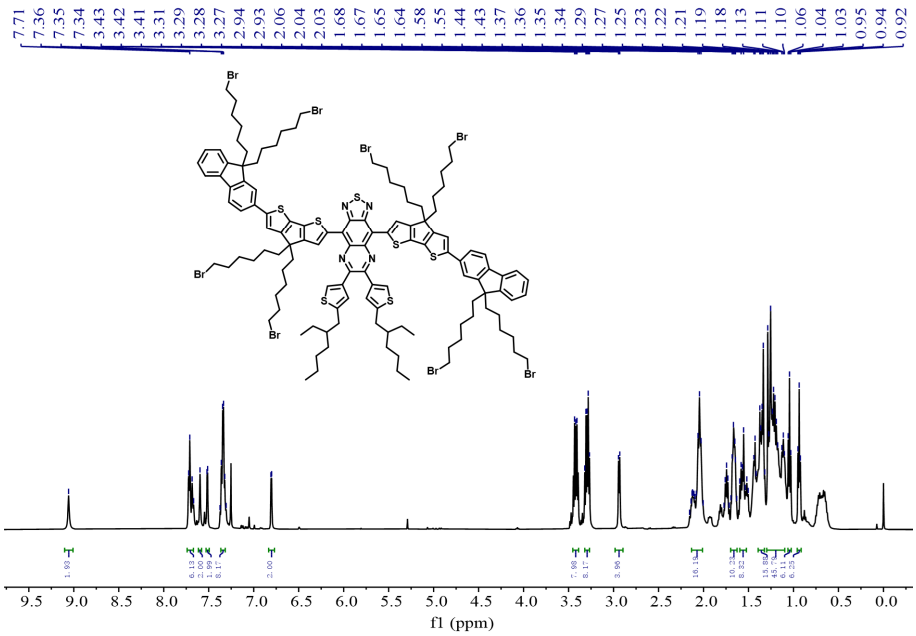


**Supplementary Fig. 13** $^{1}$H NMR spectrum of **IR-FCT.**

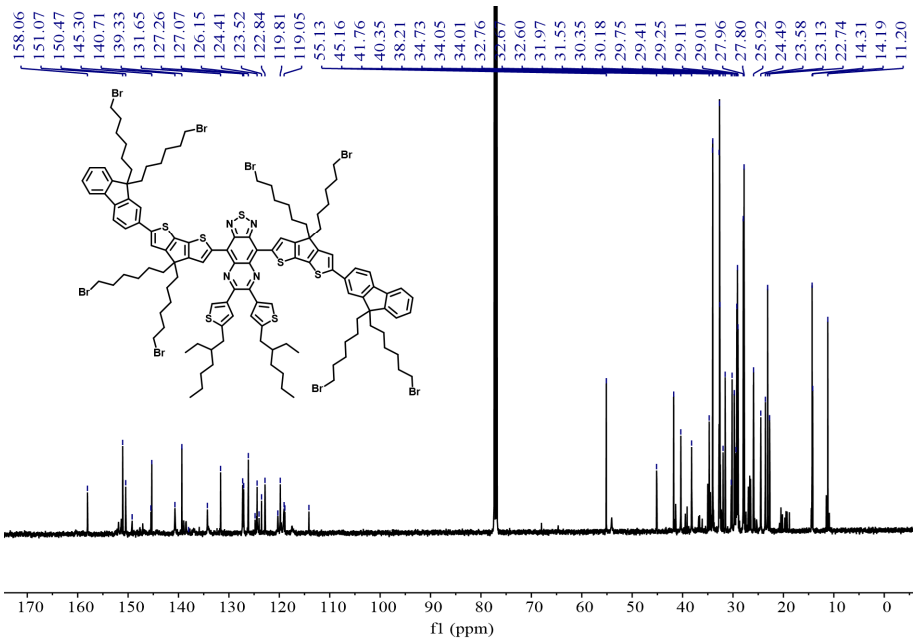


**Supplementary Fig. 14** $^{13}$C NMR spectrum of **IR-FCT**

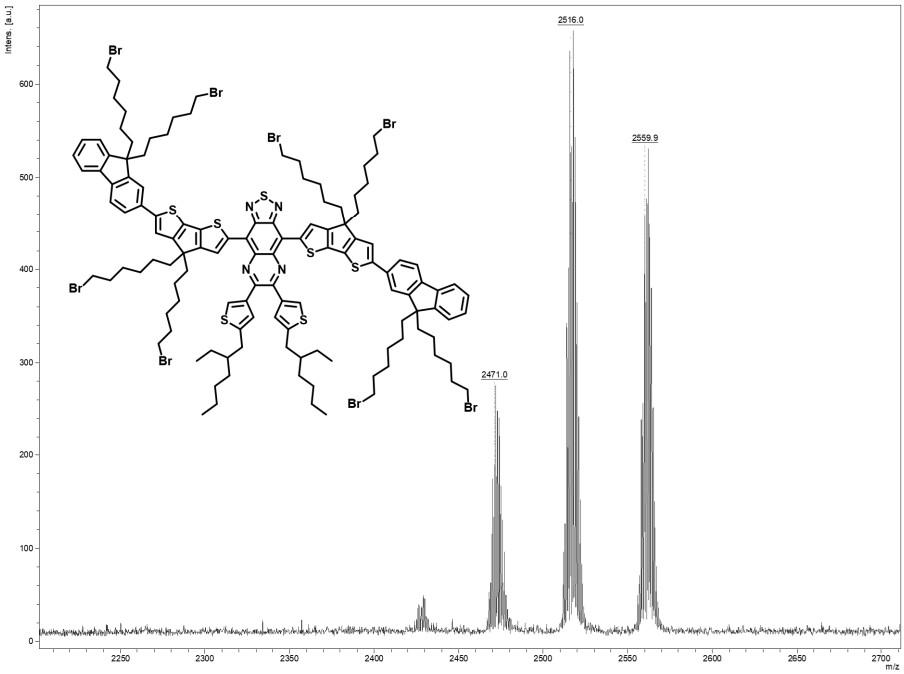


**Supplementary Fig. 15** MALDI-TOF mass spectrometry of **IR-FCT.**

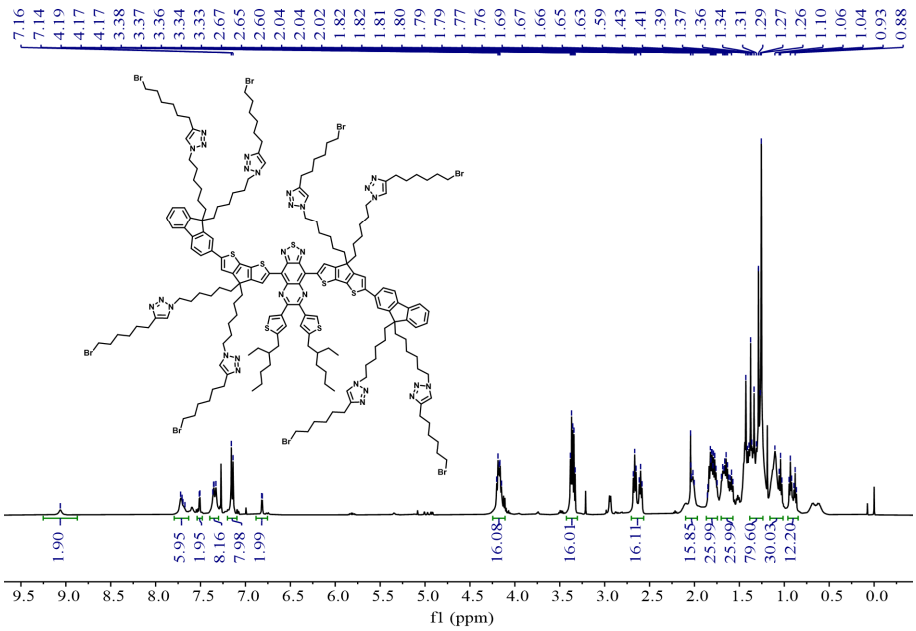


**Supplementary Fig. 16** $^{1}$H NMR spectrum of **IR-FCT8C.**

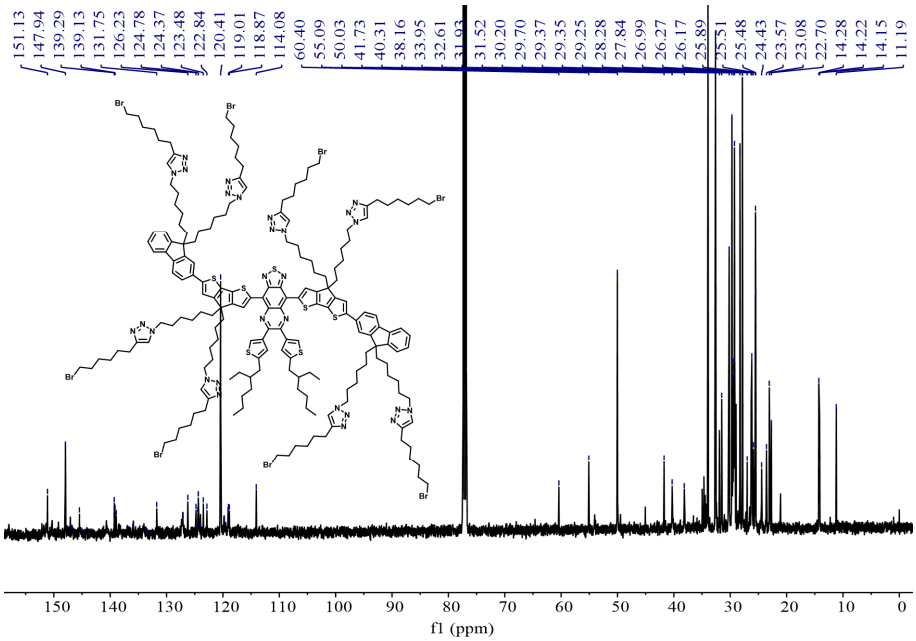


**Supplementary Fig. 17** $^{13}$C NMR spectrum of **IR-FCT8C.**

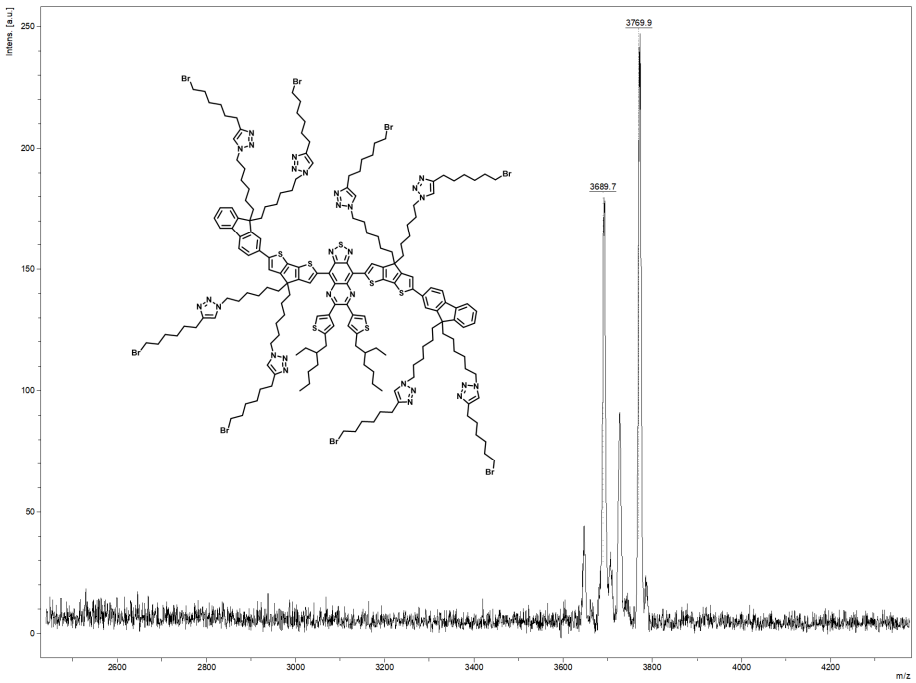


**Supplementary Fig. 18** MALDI-TOF mass spectrometry of **IR-FCT8C.**

## 5. References

[1] Yang, Q. et al. Donor Engineering for NIR-II Molecular Fluorophores with Enhanced Fluorescent Performance. *J. Am. Chem. Soc.* **140**, 1715-1724 (2018).
[2] Corrin, M., Harkins, W.D. Determination of the Critical Concentration for Micelle Formation in Solutions of Colloidal Electrolytes by the Spectral Change of a Dye1. *J. Am. Chem. Soc.* **69**, 679-683 (1947).
[3] Wang, X. et al. Unlocking the NIR-II AIEgen for High Brightness through Intramolecular Electrostatic Locking. *Angew. Chem., Int. Ed.* **63**, e202404142 (2024).
[4] Li, Z. et al. Lysosome-Targeted and pH-Activatable Phototheranostics for NIR-II Fluorescence Imaging-Guided Nasopharyngeal Carcinoma Phototherapy. *Bioconjugate Chem.* **35**, 1015-1023 (2024).
[5] Frisc, E., Frisch, M., Clemente, F., Trucks, G. Gaussian 09, Revision D. 01, Gaussian. *Inc., Wallingford CT*, (2013).
[6] Liu, F. et al. Rationally designed NIR-II excitable and endoplasmic reticulum-targeted molecular phototheranostics for imaging-guided enhanced photoimmunotherapy of triple-negative breast cancer. *J. Nanobiotechnology* **23**, 235 (2025).
[7] Yang, Q. et al. Rational Design of Molecular Fluorophores for Biological Imaging in the NIR-II Window. *Adv. Mater.* **29**, 1605497 (2017).
[8] Sun, H., Zhang, S., Zhong, C., Sun, Z. Theoretical study of excited states of DNA base dimers and tetramers using optimally tuned range-separated density functional theory. *J. Comput. Chem.* **37**, 684-693 (2016).
[9] Sun, H., Zhong, C., Bredas, J.-L. Reliable prediction with tuned range-separated functionals of the singlet–triplet gap in organic emitters for thermally activated delayed fluorescence. *J. Chem. Theory Comput.* **11**, 3851-3858 (2015).
[10] Dai, X., Chen, Y. Computational biomaterials: computational simulations for biomedicine. *Adv. Mater.* **35**, 2204798 (2023).
[11] Jiang, G. et al. Origins of near-infrared-II emission tail and fluorescence enhancement of albumin-chaperoned cyanine dyes from a multiscale computational study. *J. Mater. Chem. C* **11**, 7243-7251 (2023).
[12] Abraham, M.J. et al. GROMACS: High performance molecular simulations through multi-level parallelism from laptops to supercomputers. *SoftwareX* **1-2**, 19-25 (2015).
[13] Wang, Z., Wu, C., Liu, W. NAC-TDDFT: Time-Dependent Density Functional Theory for Nonadiabatic Couplings. *Acc. Chem. Res.* **54**, 3288-3297 (2021).